BRNO UNIVERSITY OF TECHNOLOGY
VYSOKÉ UČENÍ TECHNICKÉ V BRNĚ

CENTRAL EUROPEAN INSTITUTE OF TECHNOLOGY BUT
STŘEDOEVROPSKÝ TECHNOLOGICKÝ INSTITUT VUT

PROCESSING OF AEROGEL COATINGS ON BULK MATERIALS SUBSTRATES

PŘÍPRAVA AEROGELOVÝCH POVRCHOVÝCH ÚPRAV NA OBJEMOVÝCH MATERIÁLECH

SHORT DOCTORAL THESIS
TEZE DIZERTAČNÍ PRÁCE

AUTHOR
AUTOR PRÁCE
Jorge Alberto Torres Rodríguez

SUPERVISOR
ŠKOLITEL
prof. Ing. Jozef Kaiser, Ph.D.

BRNO 2019

ABSTRACT

In this thesis, a systematic study of the synthesis and processing of advanced thermal-stable aerogels for potential high-temperature applications was carried out. The first part of this work details the synthetic implications to prepare an aerogel and its applications along with a description of the sol-gel coatings deposition techniques. The experimental procedure is divided into three sections. The first one shows the followed synthetic protocols to prepare ZrO_2, YSZ, $Ln_2Zr_2O_7$ (*Ln* = La^{3+}, Nd^{3+}, Gd^{3+}, and Dy^{3+}) aerogels, and $Ln_2Zr_2O_7$ powders and xerogels. Then is described the used deposition method to prepare aerogel coatings on metallic substrates. Followed this, the characterization techniques are specified. It was found that the amount of water and nitric acid plays a determinant role to obtain suitable wet gels to transform into aerogels. Upon calcination at 500 °C, the ZrO_2 and YSZ aerogels have a high surface area up to 114 m^2 g^{-1}, however, at 1000 °C, complete densification occurs losing all their porous structure. In comparison with the ZrO_2 and YSZ, the $Ln_2Zr_2O_7$ aerogels are thermally more stable since preserves their porosity at elevated calcination (1000 °C) with values >160 m^2 g^{-1}. In the studied temperature range, the ZrO_2 aerogel experiment a complex tetragonal ↔ monoclinic phase transition driven by the crystallite size, while the YSZ is constituted by single-tetragonal phase. The phase composition of the rare-earth zirconates is highly dependent on the synthesis method; all the $Ln_2Zr_2O_7$ materials are pyrochlore or fluorite crystalline phases. The direct casting of the aerogel on the metallic substrate yield completely broken coatings due to effect of shrinkage, while the slurry dip-coating allowed to fabricate homogeneous, thick, and coarse aerogel coatings. These coatings do not present phase changes and remain highly porous after different heat treatments.

ABSTRAKT

Tato práce se zabývá systematickou studií syntézy a zpracováním pokročilých tepelně stabilních aerogelů pro potenciální vysokoteplotní aplikace. V první části dizertační práce jsou podrobně popsány syntetické implikace pro přípravu aerogelů a jejich aplikace spolu s popisem depozičních metod povlaků vytvořených pomocí sol-gel procesu. Experimentální postup je rozdělen do tří částí. První z nich představuje syntetické protokoly k přípravě ZrO_2, YSZ, $Ln_2Zr_2O_7$ (*Ln* = La^{3+}, Nd^{3+}, Gd^{3+}, and Dy^{3+}) aerogelů, $Ln_2Zr_2O_7$ prášků a xerogelů. Dále

je popsána depoziční metoda, která byla použita pro přípravu povlaků z aerogelů na kovových substrátech. Poté jsou následně specifikovány techniky, jež byly použity pro charakterizaci. Bylo zjištěno, že množství vody a kyseliny dusičné hraje rozhodující roli v přípravě gelů vhodných pro transformaci na aerogely. Po kalcinaci při 500 °C mají ZrO_2 a YSZ aerogely velký povrch, a to až do 114 m^2 g^{-1}, avšak při 1000 °C dochází k úplnému zhuštění a ztrácí se tak veškerá jejich porézní struktura. Naopak ve srovnání s ZrO_2 and YSZ jsou aerogely $Ln_2Zr_2O_7$ tepelně stabilnější, protože si zachovávají svou porozitu při vyšší kalcinační teplotě (1000 °C), při které dosahují hodnot > 160 m2 g-1. Experimentálně bylo dále zjištěno, že ve studovaném teplotním rozsahu ZrO_2 aerogel tvoří tetragonální komplex ↔ monoklinický fázový přechod řízený velikostí krystalitů, zatímco YSZ je tvořena jedinou tetragonální fází. Fázové složení zirkoničitanů vzácných zemin je vysoce závislé na způsobu syntézy; všechny $Ln_2Zr_2O_7$ materiály jsou pyrochlorické nebo fluoritové krystalické fáze. Přímým odléváním aerogelu na kovový substrát dochází k úplnému rozpraskání povlaku z důvodu smršťování, zatímco máčením kovového substrátu v suspenzi je možné vyrobit homogenní, silné a hrubé povlaky z aerogelu. Tyto povlaky neobsahují fázové změny a zůstávají vysoce porézní i po různých tepelných úpravách.

KEYWORDS

Soft chemistry, sol-gel, zirconates, xerogels, supercritical drying, aerogels

KLÍČOVÁ SLOVA

Soft chemistry, sol-gel, zirkoničitany, xerogely, superkritické sušení, aerogely

ACKNOWLEDGMENTS

I would like to sincerely thank all the people who helped me during my doctoral studies at the Central European Institute of Technology (CEITEC), in Brno, Czech Republic. Special mention to my supervisor Prof. Jozef Kaiser and my co-supervisor Assoc. Prof. Ladislav Čelko for opening the doors to do research in their Materials Characterization and Advanced Coatings Research Group and their invested time throughout my studies.

Deep gratitude to Ph.D. Melita Menelaou for help, guidance, and formation in the research world. Your guidance and teachings were of great help to be able to complete this research. Thank you.

My best gratefulness to all my friends and colleagues that I meet throughout these years. To my great friend of many years Mariano, your support, help, and uncountable advice was essential, not only during the Ph.D. but also in my life. Thank you.

I would like to sincerely acknowledge the CEITEC Ph.D. Scholarship and Erasmus+ program for funding my doctoral studies.

All my love and thankfulness to my parents. Your patience, support, and love were my daily motivation.

SWORN STATEMENT

I hereby declare that I have written the Ph.D. thesis on my own according to advice of my supervisor Prof. Jozef Kaiser and that all the literary sources are quoted correctly and completely. This dissertation thesis is the property of the Central European Institute of Technology (CEITEC), Brno University of Technology (BUT), Czech Republic and it can be used for commercial purposes only with consent of the doctoral thesis supervisor and the director of CEITEC, BUT.

Jorge Alberto Torres Rodríguez

TORRES-RODRIGUEZ, J. *Processing of aerogel coatings on bulk material substrates*. Brno: Brno University of Technology, Central European Institute of Technology, 2019. 123 p. Dissertation supervisor: Prof. Eng. Jozef Kaiser, Ph.D.

CONTENTS

JORGE A. TORRES RODRÍGUEZ

JorgeAlberto.TorresRodriguez@ceitec.vutbr.cz

Central European Institute of Technology · Purkyňova 656/123, C01.06 · Brno, Czech Republic, 61200 · +420 722 482 480

Central European Institute of Technology (CEITEC) Brno, Czech Republic

PhD Studies 2015-2019

EDUCATION

National Polytechnic Institute Mexico City, Mexico

MA in Advanced Technology 2014

Dissertation: "Implementation of supercritical drying equipment for aerogels production"

Autonomous University of Zacatecas Zacatecas, Mexico

BS, Chemical Engineer 2012

Dissertation: "Synthesis, characterization, and testing of TiO_2 catalysts with deposited Au nanoparticles for phenol degradation in aqueous media using the Photo-Crec-Water II reactor: effect of Au amount"

RESEARCH EXPERIENCE

Central European Institute of Technology Brno, Czech Republic

Development of materials by soft chemistry for different applications

- Design and performance of experiments to synthesize aerogels by the sol-gel method. Among others: ZrO_2, yttria-stabilized zirconia (YSZ), Lanthanide aerogels, SiO_2, TiO_2 systems.
- Development of a synthetic protocol to obtain biphasic ZrO_2 and SiO_2 aerogels with metallic Fe and Ni under a reductive atmosphere.
- Analyzed the physicochemical properties of the obtained specimens by means of SEM, EDX, XRD, TGA/DSC/MS, Raman, N_2 porosimetry.
- Optimization of a supercritical drying process to obtain aerogels in a custom-made high-pressure autoclave.
- As part of side projects, synthesis and characterization of different materials such as xerogels, powders, $CaSiO_3$ and calcium phosphates by a range of synthetic procedures such as sol-gel, co-precipitation, hydrothermal and solid-state.
- Scientific reporting and discussion, publication in peer-reviewed journals
- Write of proposals applicable to junior projects

RESEARCH INTERNSHIPS

University of Debrecen Debrecen, Hungary

October 2017-November 2017

University of Maine Le Mans, France

August 2014 – December 2014

PEER-REVIEWED PUBLICATIONS

J. Torres-Rodriguez, V. Gutierrez-Cano, M.a Menelaou, J. Kaštyl, J. Cihlář, S. Tkachenko, J. A. González, J. Kalmár, I. Fábián, I. Lázár, L. Čelko, J. Kaiser. *Inorganic Chemistry*. **2019**

J. Torres-Rodríguez, J. Kalmár, M. Menelaou, L. Čelko, K. Dvořak, J. Cihlář, J. Cihlař, J. Kaiser, E. Győri, P. Veres, I. Fábián, I. Lázár, Treatment Induced Phase Transformations in Zirconia and Yttria-Stabilized Zirconia Monolithic Aerogels. *The Journal of Supercritical Fluids*, **2019**.

M. Casas-Luna, **J. Torres-Rodríguez**; O. U. Valdés-Martínez, N. Obradović, L. Čelko. Robocasting of controlled porous $CaSiO_3$-SiO_2 structures: mechanical behavior and catalytic activity. *Ceramics International*, **Under Review.**

J. Torres-Rodriguez, M. Casas Luna, S. Tkachenko, Influence of Surfactants on SiO_2 Aerogels. *Metal 2017 Conference Proceedings*. Ostrava: Tanger Ltd., **2018.**

M. Casas Luna, S. Tkachenko, L. Klakurková, **J. Torres-Rodriguez**, T. Zikmund, Micro-Computed Tomography of Interconnected Mg-TCP Composites Obtained by Current Assisted Metal Infiltration. *Metal 2017 Conference Proceedings*. Ostrava: Tanger Ltd., **2018.**

1. Introduction

Aerogels are unusual highly porous materials because of their distinctive microstructure consisting of small pores and nanoparticles. Commonly, aerogels are prepared by means of sol-gel chemistry in three main steps: (1) formation of a colloidal suspension or also called sol, (2) transformation of the sol into a solid three-dimensional network solvent-filled or wet gel, and (3) removal of the solvent within the structure to preserve the porous structure. The final aerogel is an air-filled porous structure, usually in monolithic or powder form. In their bulk form, aerogels have interesting physical properties such as high surface area (> 100 m^2 g^{-1}) and porosity, very low thermal conductivity (~0.01-0.02 W m^{-1} K^{-1}) and density (0.003-0.5 g cm^{-3}). These properties render them in a variety of applications in both scientific and industrial fields [1]. Most of these properties exhibited in the bulk form are also transferred to different forms of the aerogels, e.g. coatings and thin sheets.

The constantly rising demand for a number of applications requires the aerogels either as freestanding sheets or as thin coatings on different substrate materials. However, certain experimental details must be taken into account to prepare aerogels in such forms since the structure of the material is naturally weak and prone to experiment damage of the produced layer. Sol-gel processes have emerged to synthesize highly pure advanced ceramics in both bulk and coating shapes.

To take advantage of the features of this material, new applications have emerged as in the energy and aerospace industries to enhance the thermal barrier coatings [2,3]. These devices require materials with low thermal conductivity and high stability to phase changes in their crystalline structure [4]. Some of these materials are yttria-stabilized zirconia (YSZ) and rare earth zirconates ($Ln_2Zr_2O_7$). Since aerogels can be prepared based on a large variety of metal oxides [5], the fusion of two novel materials such as rare-earth zirconates and aerogels for TBC applications was a great motivation for this research work. Thus, the present research details the development of a versatile synthetic methodology to produce ZrO_2, YSZ and rare earth zirconate aerogels of four lanthanides (La, Nd, Gd, and Dy) for future TBC applications. Moreover, a general study of sol-gel coatings deposition was carried out onto metallic substrates.

2. Literature review

Aerogel is an extremely porous system formed by individual nanoparticles linked in a continuous random three-dimensional network prepared by sol-gel chemistry. This synthesis protocol of inorganic aerogels involves the preparation of a colloidal suspension (sol) of metallic oxide nanoparticles in an aqueous media (alcoholic solvent). To achieve this, mainly organic precursors and metallic-based compounds which undergoes a chemical reaction are necessary; thus, producing its respective metal oxide. At the beginning of the sol-gel process, the system is in liquid state but as the reactions proceed, the nanoparticles link progressively, and the viscosity of the sol increases until it becomes a wet gel. A porous 3D network of metallic oxide filled with solvent builds this gel. Subsequently, the solvent is removed by a supercritical extraction to preserve the porous structure.

2.1. Synthesis of aerogels by sol-gel

The preparation of aerogels by sol-gel technique involves three elemental steps: (1) wet gel formation, (2) syneresis or aging, and (3) drying of the wet gel as depicted in **Fig. 2.1**.

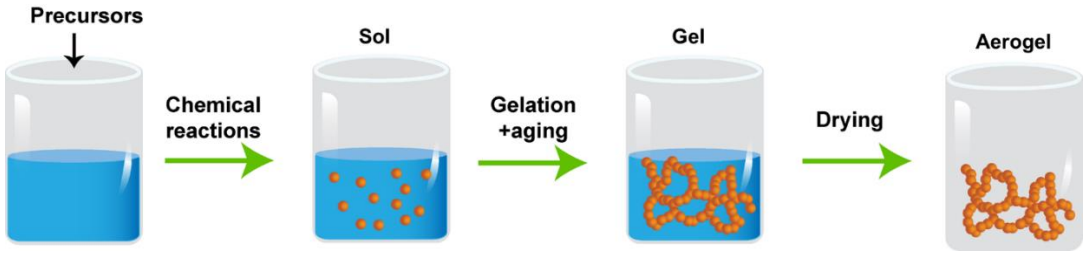

Fig. 2.1. Main steps in the synthesis of an aerogel material

2.1.1. Wet gel formation

A common way to complete the first stage is by hydrolysis and condensation reactions – also called sol-gel reactions – of alkoxides with organic solvents, water, and a catalyst. These hydrolysis and condensation reactions are strongly affected by process parameters such as the nature of the R group, the H_2O/alkoxide ratio and the catalyst. The first reaction is hydrolysis which induces the substitution of the metal-bonded alkoxy group (–OR) by a hydroxyl (-OH). The rate of the hydrolysis step depends, among others, on the nature of the alkoxide. During the condensation reactions, two M-OH groups react together and lead to the formation of metaloxane bonds. Similar to the hydrolysis, the progress of the

condensation reactions is a function of the hydrolysis degree. The length of the R chain of the alkoxide may produce inductive or steric impedance effects, which result in modification of the hydrolysis rates. Even, when highly-reactive metal alkoxides are used (i.e. Zr- or Ti-based), the use of chelating agents are necessary to reduce the very fast hydrolysis and condensation rates due the highly reactive nature of these alkoxide precursors.

2.2. Aging step

Regardless of the applied synthetic protocol to prepare a wet gel, an aging step is always needed to complete the involved reactions and strengthen the solid structure. Despite the fact that the sol loses its fluidity and turns into a rigid gel, the sol-gel reactions continue due to the oxide backbone creates the pores in the wet gel and a significant amount of unreacted species are retained into the porous structure. During the aging, that can be either in a precursor solvent or a solution [6], strengthen of the backbone network takes place.

2.3. From gel to aerogel: Drying

Once the wet gel is formed and aged, the continuous porous network is filled with solvent. The next step is to extract the solvent from the pores. However, since the wet gel is a solid – liquid system and interacts with air, there is the coexistence of solid – vapor (γ_{s-v}), liquid – vapor (γ_{l-v}), and solid – liquid interfaces (γ_{s-l}) which generates capillary pressure. Thus, if the solvent (with capillary pressure on the solid network) is evaporated while the forces are still interacting, the porous structure collapses and the result is a dense material or xerogel.

2.3.1. Supercritical drying

However, when a larger volume and very high surface area are required, the capillary forces must be avoided. In this context, gels can be dried under supercritical conditions to produce aerogels with up to 98 % of porosity by its volume. During this process, a liquid replaces the liquid filling the pores. Then, when the liquid is subjected to pressure and temperature higher than its critical point (critical pressure Pc and critical temperature Tc) the fluid is in supercritical state. A supercritical fluid has no surface tension and capillary forces are neglected and can be extracted within the pores without damaging the structure.

2.4. Aerogel applications

Being widely studied, researchers have found plenty of applications for aerogels in multidisciplinary fields. Aerogels are not only the best solid thermal insulator ever produced but also, have the lowest sound propagation in solid material and the lowest dielectric constant.

2.4.1. Applications of aerogel coatings

Most of the properties that are characteristic for bulk aerogels are also exhibited in other forms of the material, e.g., in thin sheets or films. The most frequent aerogel coatings applications are in solar cells, in ceramic transducers as acoustic impedance coatings, thermal barrier coating in infrared detectors, and sheets are used in different industrial applications such as pipes, buildings, etc.

2.4.1.1. Applications of aerogel as TBC

Taking advantage of the best characteristics of the aerogels such as low thermal conductivity and density, new applications have emerged. One of them is as a precursor material for the improvement of thermal barrier coatings (TBCs) for aerospace industry [7]. Few studies have been published attempting to apply the aerogels in a TBC system [7–9].

2.4.1.2. Yttria-stabilized zirconia

Among several types of ceramic top coats for TBCs, the 6-8 wt.% Y_2O_3 stabilized ZrO_2 (8YSZ or simply YSZ) it is the most widely used because it gathers most of the aforementioned requirements [10]. However, beyond 1200 °C, the YSZ undergoes a phase transition from non-transformable tetragonal (metastable) zirconia (t'-ZrO_2) to tetragonal (t-ZrO_2) and cubic phase (c-ZrO_2), which upon quenching, the t-ZrO_2 further transforms into monoclinic (m-ZrO_2). These phase transitions are accompanied by volume changes which might incurs in coating failure [11].

2.4.1.3. New materials as TBC precursor

Higher performance and durability requirements of gas-turbine engines will require a new generation of thermal barrier coatings. Many new TBCs materials have been proposed to achieve low thermal conductivity, high-temperature capability and higher thermal stability

of the coating systems. Thus, recent research efforts are focused on two main approaches: alternative materials and alternative stabilizers to the commonly used materials.

2.4.1.4. Rare-earth zirconates

Rare-earth zirconates ($Ln_2Zr_2O_7$; Ln is a trivalent rare-earth or lanthanide element Ln^{3+}) with pyrochlore and defect fluorite structures have attracted significant attention for high-temperature applications (>1200 °C) due to demonstrate low thermal conductivity, improved thermal stability until their melting point, good corrosion resistance, and low sintering behavior [12–14].

Aims of the doctoral thesis

The overall aim of this thesis is to carry out a systematic investigation on the synthesis and processing of advance thermal-stable aerogels for high-temperature applications. Four new aerogel materials have been selected in the form $Ln_2Zr_2O_7$ (Ln=La^{3+}, Nd^{3+}, Gd^{3+}, Dy^{3+}), along with ZrO_2 and YSZ. This work includes a study of the preparation of xerogels, aerogels, and aerogel-based coatings produced by different soft chemistry methodologies to identify the best processing routes to be applied as precursor material in future thermal barrier coatings applications. Secondary aims of the thesis are the following:

- Development of a versatile synthesis to prepare ZrO_2-based aerogels.
- Study the effect of temperature on ZrO_2 and ZrO_2-Y_2O_3 7% wt. YSZ aerogels.
- Perform a comparative study on the physicochemical properties of $Ln_2Zr_2O_7$ (Ln=La^{3+}, Nd^{3+}, Gd^{3+}, Dy^{3+}) aerogels, xerogels and powders upon heat treatment.
- Study the different deposition methodologies of aerogel coatings on metallic substrates with potential TBCs applications to be used in the future.

3. Methodology

3.1. Synthesis of aerogels

The synthesis of the studied systems is divided into three main categories: aerogels (sol-gel and supercritical drying), xerogels (sol-gel and ambient drying), and powders (co-precipitation). Six aerogel materials were synthesized (ZrO_2, YSZ, and 4 lanthanide zirconates (LZ) $Ln_2Zr_2O_7$, *Ln* = La, Nd, Gd, and Dy). To compare the physicochemical properties of the LZ aerogels, $Ln_2Zr_2O_7$, xerogels, and powders were also synthesized.

The different synthetic protocols are summarized in **Scheme 3.1**.

Scheme 3.1. Synthetic procedures followed to obtain aerogels, xerogels, and powders.

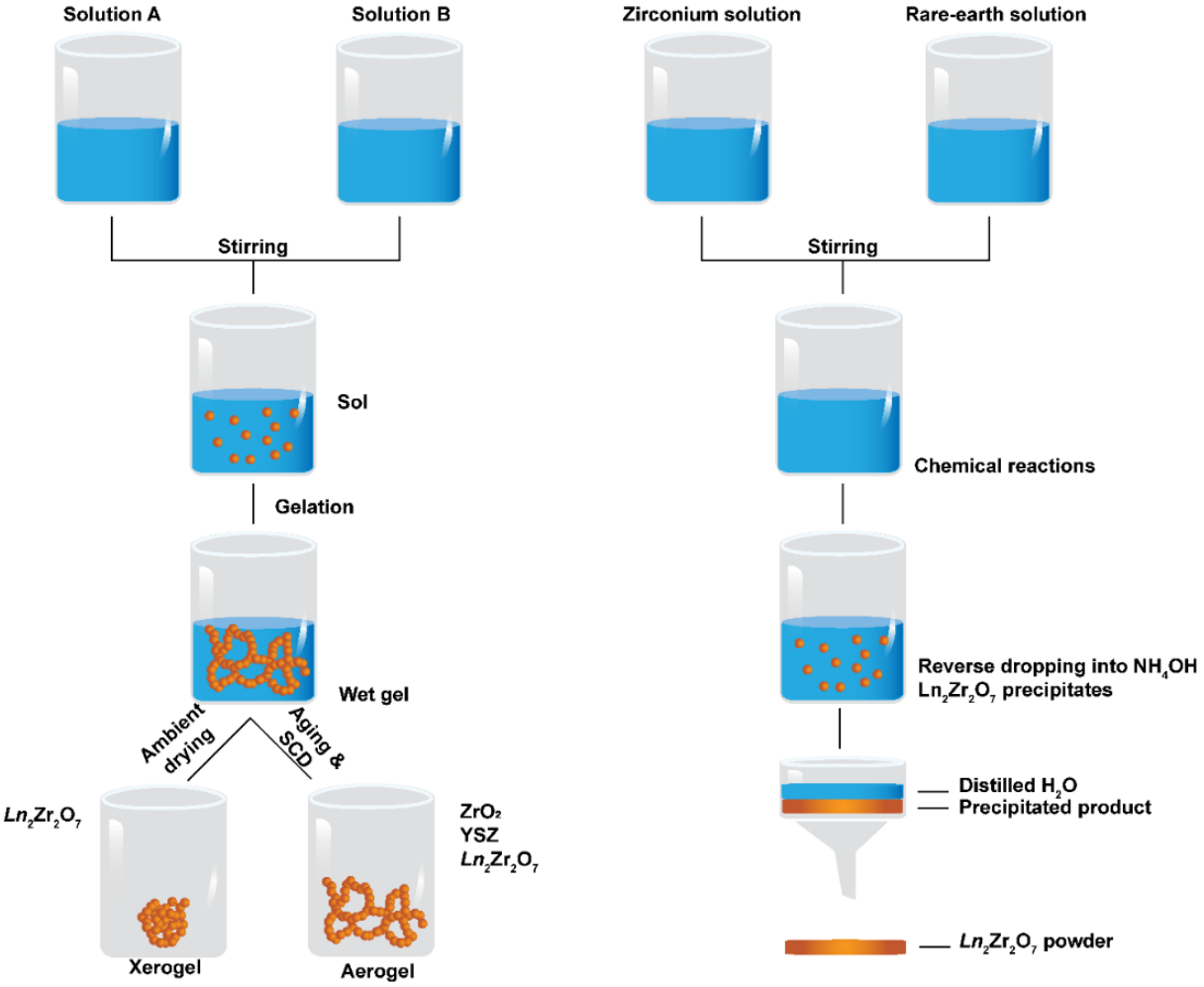

In **Table 3.1** are displayed the different synthesized materials along with their respective calcination process and sample denomination.

Table 3.1. Summary of the prepared materials and their heat treatment procedures.

Sample	Denomination	Heat treatment #1			Heat treatment #2			Heat treatment #3		
		T_1 (°C)	R_1 (°C/min)	D_1 (h)	T_2 (°C)	R_2 (°C/min)	D_2 (h)	T_3 (°C)	R_3 (°C/min)	D_3 (h)
ZrO_2 aerogel	ZrO_2-AO**	300	3	12	500	10	2	1200	10	2
YSZ aerogel	YSZ-AO**	300	3	12	500	10	2	1200	10	2
***Ln*$_2$Zr$_2$O$_7$ powders**	LnZP* LZP NZP GZP DZP	120	3.3	12	1000	3.3	5	---	---	---
***Ln*$_2$Zr$_2$O$_7$ Xerogels**	LnZX* LZX NZX GZX DZX	120	3.3	12	1000	3.3	5	---	---	---
***Ln*$_2$Zr$_2$O$_7$ aerogels**	LnZA* LZA NZA GZA DZA	120	3.3	12	1000	3.3	5	---	---	---

T: temperature set point; R: used heating ramp; D: dwell time.

* *Ln* = La^{3+}, Nd^{3+}, Gd^{3+}, Dy^{3+}. The denomination was set with L for lanthanum, N for neodymium, G for gadolinium, and D for dysprosium; P for powders, X for xerogels, and A for aerogels (i.e. LnZA, and NZA corresponds to lanthanide zirconate aerogels, and Neodymium zirconate aerogel, respectively).

** The –AO stands for as-obtained samples.

3.2. Deposition of aerogel coatings

Coatings were prepared onto two different metallic substrates: 20x20x5 mm 99.5 Al, and Ø 10 mm cylindrical and 10 mm in thickness Ni-based MAR-M-247 alloy. To enhance surface coarsening, prior deposition, the substrates were grit blasted using Al_2O_3 particles with the aim to increase the surface roughness and improve the coating adhesion. Then, surface treated substrates were ultrasonically cleaned in acetone for 30 minutes and dried by a flow of nitrogen.

Different coating deposition methods were investigated in detail: doctor blade, dip coating, and slurry dip-coating (**Fig. 3.1**).

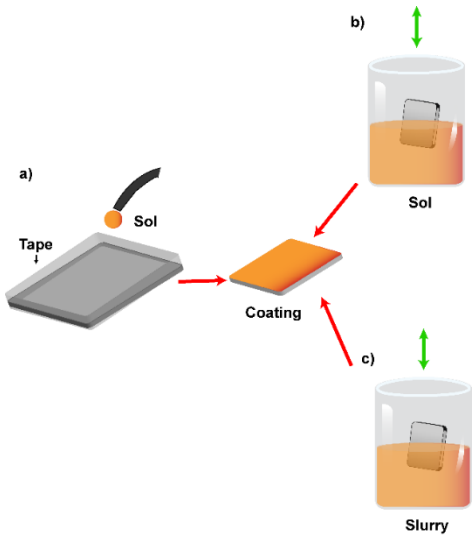

Fig. 3.1. Different employed deposition methods; a) doctor blade casting; b) dip-coating into a precursor sol, the sol further turned a wet gel layer which was dried under supercritical conditions; c) dip-coating into a slurry composed of aerogel as dispersed powder and the original sol as liquid media.

3.3. Characterization

3.3.1. Microstructural study

To investigate the surface morphology of the materials and coatings, a high-resolution scanning electron microscope (HR-SEM) 460L Verios (FEI, Czech Republic) was used. Prior SEM studies, the samples were prepared on a carbon tape followed by a deposition of a conducting thin carbon layer.

3.3.2. Porosity

The specific surface area as well as the pore size and distribution of the materials were determined in an Autosorb iQ (Quantachrome Instruments, Boynton Beach, FL, USA) sorption analyzer at 77.4 K. The samples were degassed in vacuum at 180 °C for 12 hrs. Specific surface area (S_{BET}) was calculated by using the Brunauer-Emmett-Teller (BET) method [15]. The micropore volume and micropore area were calculated using the t-plots (De Boer) method [16]. The pore size distribution of the samples was determined from the desorption isotherms using the Barrett-Joyner-Halenda (BJH) model [17].

3.3.3. Phase analysis

XRD patterns from all samples were recorded using an X-ray diffractometer (Rigaku, Japan). A Cu-K_α radiation source (λ = 1.5406 Å) was used as the X-ray source. The XRD patterns were collected from 10 to 90° or in some specific cases from 20 to 65°C. To identify the systematic phase transition of ZrO_2 and YSZ samples, *in-situ* X-ray diffraction was performed. The samples were heated from 25 up to 1200 °C. Each 100 °C a pattern was recorded from 22 to 37°. Quantitative phase analysis was realized according to the Rietveld method. Crystallite size (D) was determined from the X-ray line broadening using Scherrer's equation (Eq. 3.1):

$$D = \frac{K\lambda}{\beta cos\theta} \qquad \textbf{(Eq. 3.1)}$$

where K is the shape factor (assumed spherical shapes; 0.89), λ is the X-ray wavelength (0.154 nm), β is the line broadening at half of the maximum intensity in radians (full width at half maximum: FWHM), and θ is the Bragg angle.

3.3.4. Spectroscopy

Raman spectroscopy was used to assign accurately the present crystalline phases in the bulk $Ln_2Zr_2O_7$ powders, xerogels, and aerogels. Non-polarized Raman spectra were acquired in backscattering geometry with a Horiba T64000 Raman spectrometer equipped with a triple monochromator in the subtractive configuration (spectral resolution of 0.6 cm^{-1}) coupled to a confocal microscope.

3.3.5. Furnace cycle oxidation test (FCT)

The $La_2Zr_2O_7$ coatings prepared by the slurry dip-coating were tested in the Rapid Temp Model 1612 BL laboratory box furnace with cycling package (CMfurnaces, USA). The samples were placed on the ceramic platform and subsequently heat-treated. The testing conditions of FCT included (i) the heating ramp of 77 °C/min to reach a working temperature of 1100 °C, (ii) 60 min dwell time at the temperature and followed by (iii) fan cooling of the samples for 15 min.

4. Results and discussion

For applications of aerogels in high-temperature coatings, the physicochemical properties of the aerogel to deposit are important, as it is the deposition methodology. A complete assessment of six aerogels is discussed (zirconia (ZrO_2), yttria-stabilized zirconia (YSZ), and rare earth zirconates $Ln_2Zr_2O_7$ (Ln = La^{3+}, Nd^{3+}, Gd^{3+}, and Dy^{3+}). In addition, $Ln_2Zr_2O_7$ xerogels and powders were prepared and characterized. Finally, a study of different deposition methods of aerogels was carried out.

4.1. ZrO_2 and YSZ aerogels: Synthesis and characterization

The development of a synthetic protocol to prepare ZrO_2 aerogels and that can be practical for other Zr-based aerogels was performed. These experiments were conducted under acidic conditions with HNO_3. The optimized parameters yield monolithic ZrO_2 and YSZ aerogels.

4.1.1. Mechanism of formation of Zr-based aerogels

The formation of Zr-based aerogels is driven by the hydrolysis rate of the propoxide which is function of the acid concentration. The first step is the protonation of the alkoxy group (**Scheme 4.1**) to form the hydroxyl group (-ROH). Eventually, a completely hydrolyzed transition complex is formed (denoted as Hydr-Zr). If the acid concentration [H^+] is high, it might protonate a hydroxyl group of the Hydr-Zr complex to form the transition complex Prot-Zr. To understand the role of acid concentration is necessary to observe **Scheme 4.2** and **Table 4.1**. From these results, can be noticed that at HNO_3 below 0.1 mL, precipitation occurs and above 0.4 mL the gelation is suppressed. These results are correlated to the acid concentration.

Scheme 4.1. The molecular mechanism of the acid-catalyzed hydrolysis of the Zr(IV) precursor leading to the formation of ZrO_2 and YSZ wet gels[18].

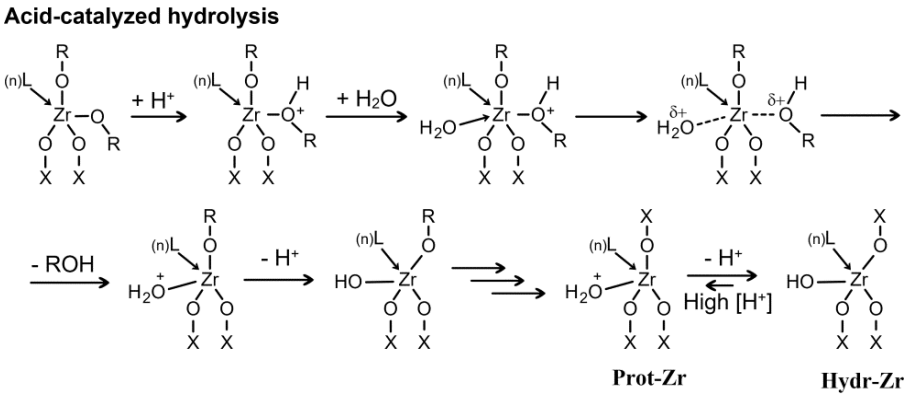

where R = n-C_3H_7, X = H or Zr, L = n-C_3H_7OH or H_2O, n = 1 - 4

At moderate acid concentrations (@Moderate [H+]) the condensation reactions are completed by H_2O and alcohol molecules which takes place in parallel (**Scheme 4.2**). Thus, the formation of bridging Zr-O-Zr in the zirconia network takes place. If the acid concentration is higher (@Medium [H^+]), the protonated complex Prot-Zr is involved in the water condensation process. However, when the acid concentration is too high (@High [H^+]) the majority of the complexes are in the protonated form (Prot-Zr), therefore there is a substantial decrease of the active Hydr-Zr complex, which leads diminishing in the reactions rates and the condensation is inhibited.

Table 4.1. Experimental conditions used to prepare samples ZrO_2-1, ZrO_2-2 and ZrO_2-3. ZrO_2-1: (@Moderate [H+]; ZrO_2-2: (@Medium [H+]; ZrO_2-3: (@High [H+].

Sample	$Zr(OPr)_4$ [mL]	1-propanol [mL]	HNO_3 [mL]	H_2O [mL]	*Tg*[a)] [min]	Resultant gel
ZrO_2-1	1	10	<0.1	0.05	NA	Precipitate
ZrO_2-2	1	10	0.1	0.05	10	Light white gel
ZrO_2-3	1	10	>0.4	0.05	NA	No gelation

a)Gelation time

Scheme 4.2. Sol-gel reactions of ZrO_2 aerogels; a) proposed mechanism for the formation of ZrO_2 nanoparticles and colloidal particles (sol) under different acidity conditions. b) The representation of the assembly of primary and secondary globules to a self-supported wet gel structure [18].

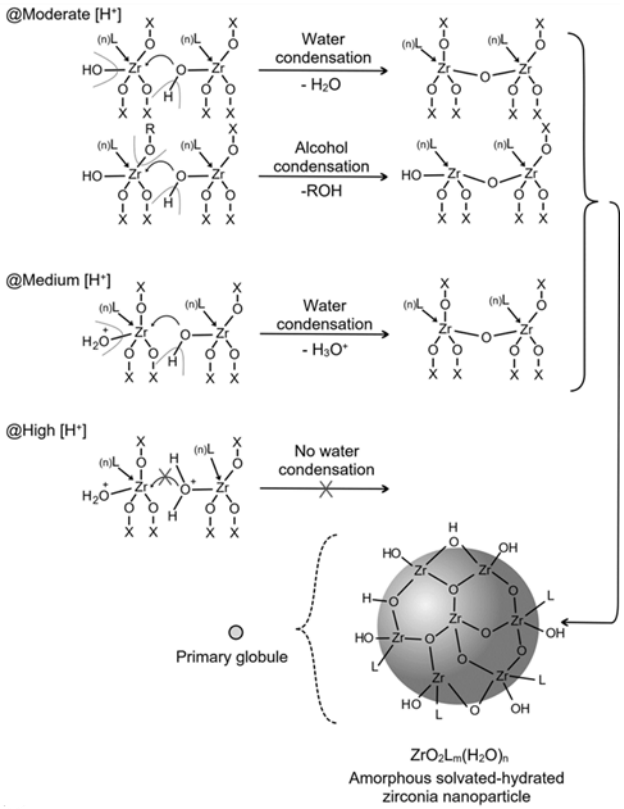

4.2 Characterization of ZrO_2 and YSZ aerogels

For high-temperature porous coatings applications, the structural changes upon heat treatment are important. To investigate the physicochemical properties of the as-obtained aerogels (i.e. ZrO_2-AO and YSZ-AO), a systematic study was carried out.

4.2.1 Effect of temperature on the aerogels properties

In **Table 4.2** can be observed that the ZrO_2-AO aerogel has a specific surface area (S_{BET}) of 255 $m^2\,g^{-1}$ and a pore volume (V_p) of 2.1 $cm^3\,g^{-1}$. Upon calcination at 500 °C, these values decreased to 87 $m^2\,g^{-1}$ and 0.7 $cm^3\,g^{-1}$ representing a reduction of 66% and 31% for S_{BET} and V_p respectively. The YSZ-AO aerogel has a S_{BET} of 243 $m^2\,g^{-1}$ and a V_p of 1.6 $cm^3\,g^{-1}$. After calcination, resulted in a drop of the S_{BET} to 114 $m^2\,g^{-1}$ (54%) while the V_p remained unchanged. Characteristic pore sizes are nearly identical for the as-obtained samples, and only moderately decrease upon heating at 500 °C. The change of the total pore volume upon heat treatment indicates the shrinkage degree, which can be a reference criterion on the

dimensional stability of the aerogels that in coatings for high-temperature applications is important due to the densification of the material. In this regard, the ZrO_2-AO aerogel experiences a significant decrease in V_p since its value fall by 31% after heat treatment. In contrast, the V_p of the YSZ aerogel does not change upon calcination at 500 °C / 2hrs which demonstrates that the YSZ aerogel is less susceptible to dimensional changes upon calcination. Samples were also treated at the temperature of 1200 °C, however, at such conditions, the samples showed high densification degree and consequently, closing the open pores which resulted in values below 1 m^2 g^{-1}.

Table 4.2. Textural properties of the ZrO_2 and YSZ aerogels before and after calcination. Standard deviations are displayed for primary data.

Sample	S_{BET} $[m^2 g^{-1}]$[a)]	Vp $[cm^3 g^{-1}]$[b)]	$V_{mesopore}$ $[cm^3 g^{-1}]$[c)]	$V_{macropore}$ $[cm^3 g^{-1}]$[d)]	Dp (nm)[e)]	$D_{p\text{-}avg}$ (nm)[f)]	C-const.[g)]
ZrO_2-AO	255 ± 21	2.1 ± 0.2	1.4	0.71	47	33	39
ZrO_2-500	87 ± 13	0.7 ± 0.1	0.46	0.19	46	31	86
YSZ-AO	243 ± 14	1.6 ± 0.1	1.1	0.54	45	27	57
YSZ-500	114 ± 19	1.6 ± 0.3	1.3	0.35	37	56	83

[a)] BET specific surface area; [b)] Total pore volume; [c)] Pore volume of mesopores; [d)] Pore volume of macropores; [e)] Characteristic pore diameter: estimated at the maximum of the distribution curve; [f)] Average pore size: estimated by BJH method; [g)] Constant value as an indicator of the polarity of the sample surface [15,19].

Microstructural and morphological changes before and after calcination at 500 °C / 2 hrs were also investigated. From **Fig. 4.1** is appreciated that the as-obtained samples have the characteristic aerogel microstructure built by aggregates of nanosized particles with no apparent differences between them. After heat treatment at 500 °C, the surface of the ZrO_2-500 sample shows some open pores and the particle aggregates are smaller due to densification. This can be related to the decrease in the pore volume of the ZrO_2-500 (**Table 4.2**). The surface of the YSZ-500 is coarser containing larger aggregates. In both samples, at 1200 ºC, the particles grow considerably and dense agglomerates are formed which is indicative of an extensive sintering process (**Table 4.2)**.

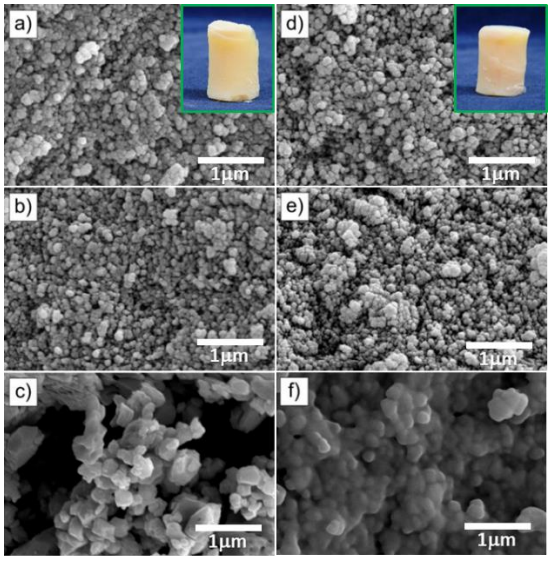

Fig. 4.1. SEM images of the ZrO_2 and YSZ aerogels before and after the heat treatment: a) ZrO_2-AO, b) ZrO_2-500, c) ZrO_2-1200, d) YSZ-AO, e) YSZ-500 and f) YSZ-1200. Insets: photographs of the ZrO_2-AO and YSZ-AO monoliths, respectively [18].

According to the phase composition and crystallite size as function of the temperature determined by *in-situ* XRD, a correlation between both components was investigated (**Fig. 4.2** and **Fig. 4.3**). Based on the obtained results the tetragonal phase can exist only if the aerogel contains nanometer-sized crystallites. First, the amorphous ZrO_2 transforms into a t-ZrO_2 phase (crystallite size: 6.0 – 13.6 nm) in a thermodynamically controlled process that finishes at ca. 800 ºC. As the temperature increases to 900 ºC, the crystallite size approaches the critical size of t-ZrO_2 of 30 nm and the thermodynamic stability of the tetragonal and monoclinic phases become comparable. This results in a tetragonal-to-monoclinic phase transformation which becomes clearly visible at 1000 ºC where the critical crystallite size is reached (31.7 nm). The temperature component becomes dominant again close to the monoclinic-to-tetragonal phase transformation temperature of 1170 ºC. Subsequent heating at 1200 ºC leads to the complete transformation to a pure tetragonal phase.

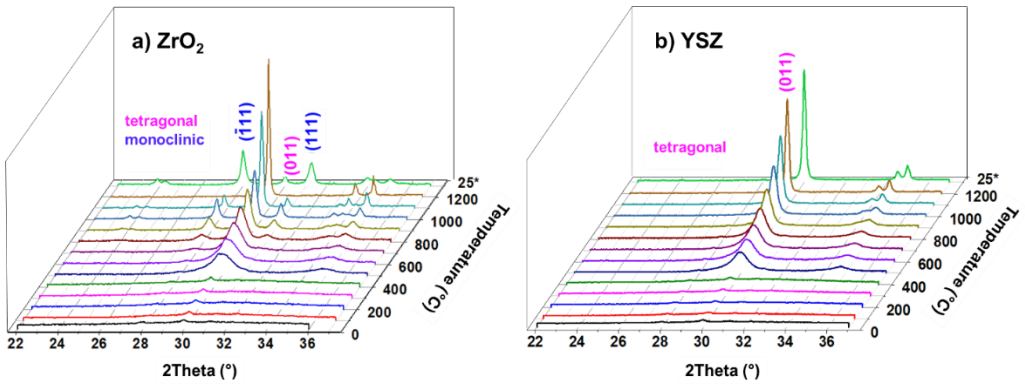

Fig. 4.2. Temperature-dependent XRD patterns of a) ZrO_2 and b) YSZ aerogels. In-situ XRD measurements from 25 to 1200 °C were performed during the calcination of the amorphous aerogels in order to determine their crystallographic evolution. The last pattern (25^*) was recorded upon quenching [18].

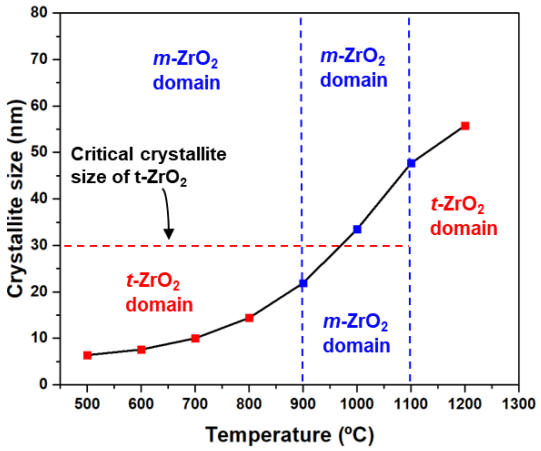

Fig. 4.3. Effect of temperature on crystallite size observed during the heat treatment of ZrO_2-AO aerogel. Crystallite size was calculated from in-situ XRD data (see **Fig. 4.2**) [18].

The developed synthetic route to produce Zr-based aerogels intended for high-temperature coatings applications, yields high-quality bulk aerogels. All these studied properties are transferred from the bulk to the coating form. Namely, the temperature reduces considerably the porosity and therefore shrinks the material up to 60 % as in the case of the ZrO_2. However, the YSZ aerogel demonstrated lesser shrinkage degree and enhanced phase stability since single-phase tetragonal zirconia was present from the room temperature up to 1200 °C.

4.3. $Ln_2Zr_2O_7$ (Ln=La^{3+}, Nd^{3+}, Gd^{3+} and Dy^{3+}) aerogels: Synthesis

A variant of the previously described synthetic protocol for ZrO_2/YSZ aerogels synthesis was tailored to be able to prepare 4 rare-earth zirconate aerogels ($Ln_2Zr_2O_7$; *Ln* = La^{3+}, Nd^{3+},

Gd^{3+}, and Dy^{3+}). Such studies do not exist in the literature. Since such aerogels (LnZA) were prepared for the first time, conventional powders (LnZP), and the aerogels' counterpart xerogels (LnZX) were prepared by co-precipitation and sol-gel method, for comparison purposes, respectively. Upon preparation, physicochemical characterization was performed to all the studied systems.

4.3.2 $Ln_2Zr_2O_7$ materials characterization: powders, xerogels, and aerogels

In comparison with the ZrO_2 and YSZ aerogels with a mixture of tetragonal and monoclinic zirconia or single-phase tetragonal respectively, the LZ materials presented a cubic crystalline structure consistent to the Miller indices (222), (400), (440), (622), and (444) which can be assigned to cubic phase with either ordered pyrochlore (P) or disordered fluorite (F) structures (**Fig. 4.4**). Since the characteristic diffraction peaks of the pyrochlore structure located at 2θ on 36° and 45° oriented in (331) and (551) were not observed to discern between F or P structures [20], further analysis were performed by Raman spectrometry.

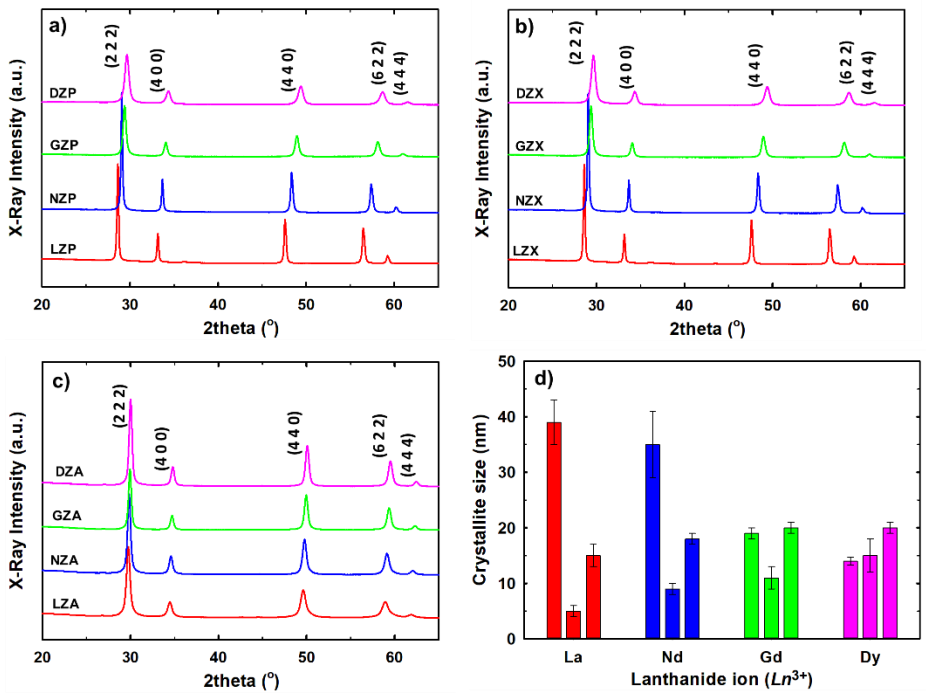

Fig. 4.4. X-ray diffraction patterns of the calcined materials at 1000 °C: a) powders (LnZP); b) xerogels (LnZX); c) aerogels (LnZA) and d) calculated crystallite size as a function of the lanthanide ion (Ln^{3+}). For each element, from left to right, each bar corresponds to LnZP, LnZX, and LnZA, respectively [21].

The difference between the pyrochlore and fluorite structures in $Ln_2Zr_2O_7$ compounds is that the pyrochlore structure has 6 Raman active modes (**Eq. 4.1**) in the center of the Brillouin zone, while the fluorite structure is characterized by a single Raman active mode (F_{2g} located at approx. 466 cm^{-1}) [22,23].

$$\Gamma = A_{1g} + E_g + 4F_{2g} \qquad (\boldsymbol{Eq.4.1})$$

The LZP and NZP (**Fig. 4.5a-b)** presented the A_{1g} (514 cm^{-1}; bending O-Zr-O), the E_g (297 cm^{-1}; Zr-O), and the F_{2g} (391 and 495 cm^{-1} assigned to La-O and Zr-O, respectively) modes [24–26]. Thus, ordered pyrochlore structure (Fd3m) was determined in the both samples. The GZP and DZP samples follow similar patterns among them (**Fig. 4.5c-d**) and are constituted by fluorite structure with some order at the microdomain levels [26]. The LZX and NZX contain only pyrochlore structure (**Fig. 4.5e-f**) and the GZX and DZX (**Fig. 4.5g-h**) are composed of mainly fluorite with some amount of pyrochlore structure. All the synthesized aerogels (**Fig. 4.5i-l**) have a mixture of $Ln_2Zr_2O_7$ and t-ZrO_2.

Since both systems were prepared with the same composition (ambient drying and supercritical drying for xerogels and aerogels, respectively), these results suggest that the drying process has an influence in the final crystalline structure of the prepared materials [27–30]. The combination of XRD and Raman spectroscopy shows the change of structure in LnZP and LnZX nanostructured materials when replacing the *Ln* site by either La^{3+}, Nd^{3+}, Gd^{3+}, or Dy^{3+} cations, leading into a transformation from ordered pyrochlore structure to a disordered fluorite structure with a certain order at the microdomains. The tendency to have disordered structure increases with moving from La^{3+} to Dy^{3+} in the lanthanide series.

The differences on the microstructure can be seen in **Fig. 4.6a**. The LnZP are formed by a dense surface of grain sizes of ~100 nm with a random orientation. On the other hand, the xerogels (**Fig. 4.6b**) are composed of spherical particles of ~100 nm. These aggregated particles are roughly consolidated upon calcination. However, despite the consolidation, a highly porous material was obtained in comparison with LnZP. Interestingly, despite the calcination, the aerogels showed the typical morphology of this type of material, which is built by aggregated spherical particles (~ 70 nm) with large extent of open porosity, distributed along the surface (**Fig. 4.6c**). The aerogels do not show any consolidation of the particles/aggregates that demonstrates excellent resistance upon thermal sintering.

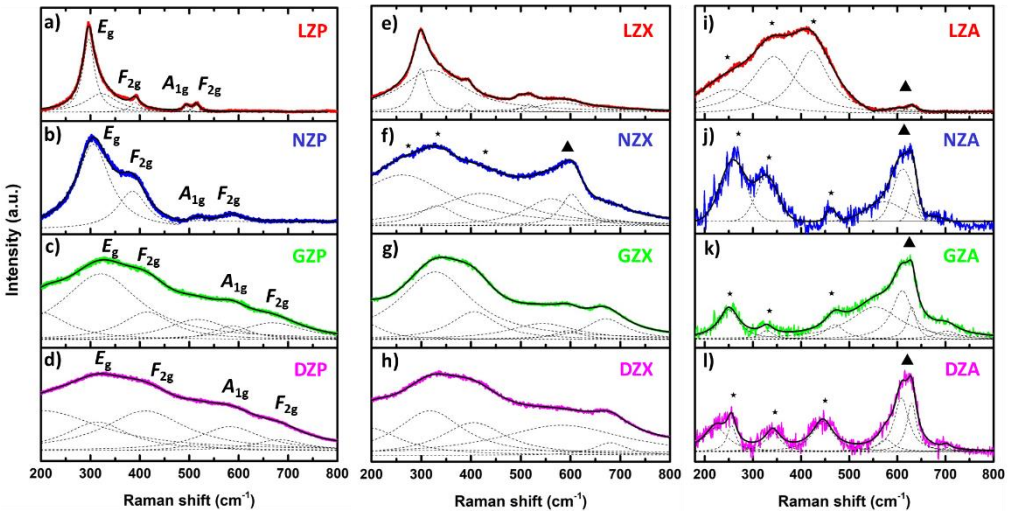

Fig. 4.5. Raman spectra of the LZ materials at ambient conditions: a-d) LnZP, e-h) LnZX, i-l) LnZA. Vibrational modes of tetragonal zirconia are depicted with stars (*) and vibrational modes of LnZ cubic phase are depicted with triangles (▲) [21].

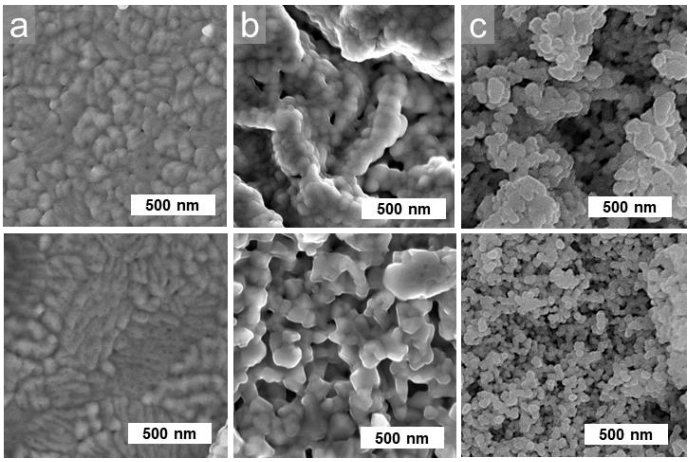

Fig. 4.6. Scanning electron microscopy: Surface morphology of the calcined $La_2Zr_2O_7$ and $Gd_2Zr_2O_7$ powders (LnZP) (a), xerogels (LnZX) (b) and aerogels (LnZA) (c) at 1000 °C/5h. Additional SEM pictures are shown in Appendix A [21].

The specific surface areas (S_{BET}) are summarized in **Table 4.3**. In general, the materials with the largest surface areas are the LnZX and LnZA, specifically, the DZX and GZA with values of 144 and 168 m^2g^{-1}, respectively, whereas the LnZP showed to be quite dense materials with surface areas < $1m^2g^{-1}$. However, the values reported in **Table 4.2** for the ZrO_2 and YSZ aerogels (in the order of 80-114 m^2g^{-1}), are somewhat comparable with surface areas of around 100-168 m^2g^{-1} of those of the LnZA. Even, it can be considered that the LnZA have a better resistance against the consolidation of the particles (and shrinkage) since the ZrO_2/YSZ were calcined at 500 °C for 2 hours and those of LnZA at 1000 °C for 5 hours.

Table 4.3. Summary of N_2 sorption analysis of calcined samples [21].

Sample	S_{BET} (m^2g^{-1})	C value	Micropore area (m^2g^{-1})	Micropore volume (cm^3g^{-1})	Pore diameter average (nm)	Pore diameter characteristic* (nm)	Total pore volume (cm^3g^{-1})
LZP	0.9	42 ± 4	0.2	0.000	-	-	0.010
NZP	0.3	12 ± 1	0.1	0.000	-	-	0.001
GZP	0.3	7 ± 1	0.1	0.000	-	-	0.001
DZP	0.4	5 ± 2	0.1	0.000	-	-	0.001
LZX	124 ± 18	162 ± 16	121	0.062	2.1	1.7	0.066
NZX	129 ± 19	111 ± 10	126	0.063	2.1	1.7	0.067
GZX	85 ± 12	129 ± 13	80	0.039	2.4	1.7	0.051
DZX	144 ± 19	128	142	0.068	2.0	1.7	0.071
LZA	100 ± 10	89 ± 8	-	-	40.0	120	1.0
NZA	102 ± 11	103 ± 9	-	-	39.9	110	1.02
GZA	168 ± 16	66 ± 6	-	-	36.5	131	1.53
DZA	139 ± 14	74 ± 6	-	-	35.2	119	1.22

* Characteristic pore diameter: estimated at the maximum of the distribution curve

The physicochemical properties and crystallinity of the synthesized materials are highly dependent on the synthetic protocol. The co-precipitation method resulted in highly densified materials with surface areas below 1 m^2g^{-1} while the sol-gel yield highly porous networks built by aggregates of nanoparticles with high specific surface area in the order of 130 m^2 g^{-1} upon calcination at 1000 °C / 5hrs. Those values are larger than the ZrO_2 and YSZ aerogels that after calcination process experimented high densification that resulted in a dramatic drop of their specific surface area (below 1 m^2 g^{-1}). Such calcination process developed the evolution of $Ln_2Zr_2O_7$ structure with either ordered pyrochlore structure (LZP, NZP, LZX, NZX), and disordered fluorite (GZP, DZP, GZX, and DZX). On the other hand, the aerogels are mainly composed of $Ln_2Zr_2O_7$ structure with traces of t-ZrO_2. As comparison, a mixture of m-ZrO_2/t-ZrO_2 and t-ZrO_2 constituted the ZrO_2 and YSZ aerogels, respectively.

4.4. Preparation of aerogel-based coatings by soft chemistry deposition techniques

4.4.1. Doctor-blade: tape casting

In these series of samples, the thickness of the coating was varied by the dropped volume of sol onto the substrate; samples with low sol volume and low thickness of 125 μm (hereafter 125YSZ) and thicker samples with a larger amount of deposited sol with average coating

thickness of 250 μm (250YSZ). To avoid damaging of the aerogel coating during the supercritical drying process, the samples were set parallel to the CO_2 flow.

The 250YSZ sample (**Fig. 4.7c, f**) is constituted by fragmented pieces of aerogel which are barely coating the surface and large non-coated portions are visible. On the contrary, 125YSZ sample (**Fig. 4.7e**) is almost completely covered, although there is some detachment on the edges. Cracks of some tens of microns are propagated on the coating.

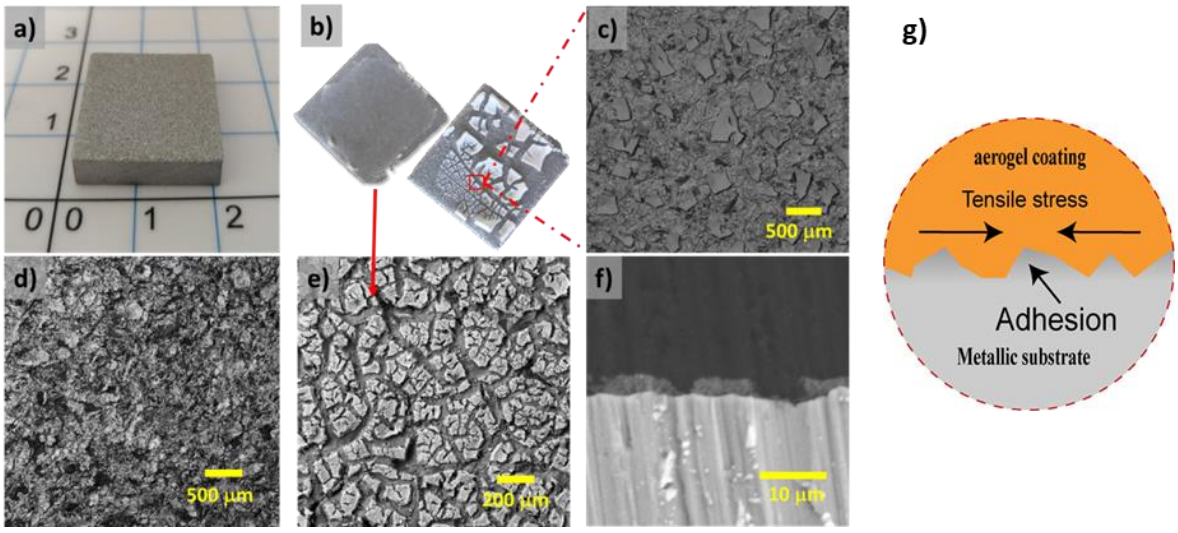

Fig. 4.7. Surface morphology of the doctor-blade coatings; a) square aluminum grit blasted substrate before deposition; b) 125YSZ (upper left), 250YSZ (down right); c) surface morphology of the 250YSZ sample; e) surface morphology of the 150YSZ sample; f) cross-section of the 150YSZ sample; g) generated tensile stress produced during the aerogel coating shrinkage.

Both, the spallation on the edges, and the presence of cracks are related to the irreversible shrinkage of aerogels which takes place during the CO_2 extraction. Directly upon supercritical drying, the aerogel coatings shrunk ~30 % and ~10 % for 250YSZ and 125YSZ respectively. It has been reported that when the aerogel coating is adhered to the surface (**Fig. 4.7g**), upon shrinkage, tensile stress is generated [31,32].

4.2.2. Dip-coating: sol approach

The coatings were obtained using solutions at different aging times due the viscosity increase with the aging [33,34]. Thus, the substrates were dipped after 1 and 2.5 minutes after sol preparation. The wet gel coatings were then supercritically dried. The coatings obtained after 1 minute (**Fig. 4.8a**) are formed by small pieces of aerogel that do not cover the entire

surface. In contrast, the surface of the more aged sample (**Fig. 4.8b**) is noticeably more homogeneous and the aerogel layer covers most of the substrate. These cracks are effect of the tensile stress generated by the contraction of the coating upon drying. In fact, it can be found in the literature that only very thin coatings below 5 μm are free or cracks [35–37].

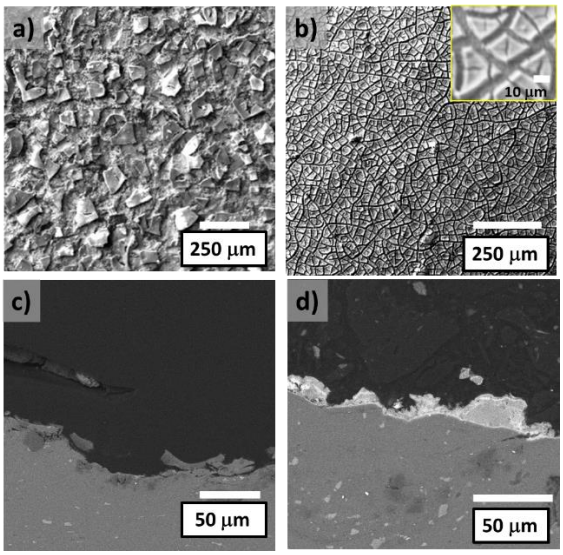

Fig. 4.8. Coatings prepared by the sol-gel coating varying the aging period of the precursor sol; a) surface of the coating after 1 min; b) surface of the coating after 2.5 min; c) cross-section of the coating after 1 min; d) cross-section of the coating after 2.5 min.

4.2.3. Dip-coating: slurry

The samples were prepared on MAR-M-247 Ni-based alloy substrates. For this deposition, substrates were continuously dipped in a slurry composed of $La_2Zr_2O_7$ aerogel powder dispersed in its original sol. After each deposition, the coating was dried at 50 °C for 5 min. The studied variables were: the powder loading (10-30% wt.) and the number of deposits (1-3).

In general, the 10 %wt. slurry produced coatings formed by aerogel aggregates of ~50 μm (**Fig. 4.9a-c**). As the number of deposits increase, a slight coarsening of the surface can be noticed. Uncoated zones were revealed as blue spots (aluminum) by the EDX images (**Fig. 4.9g-i**) in all the samples. This is the result of low amount of dispersed powder into the slurry.

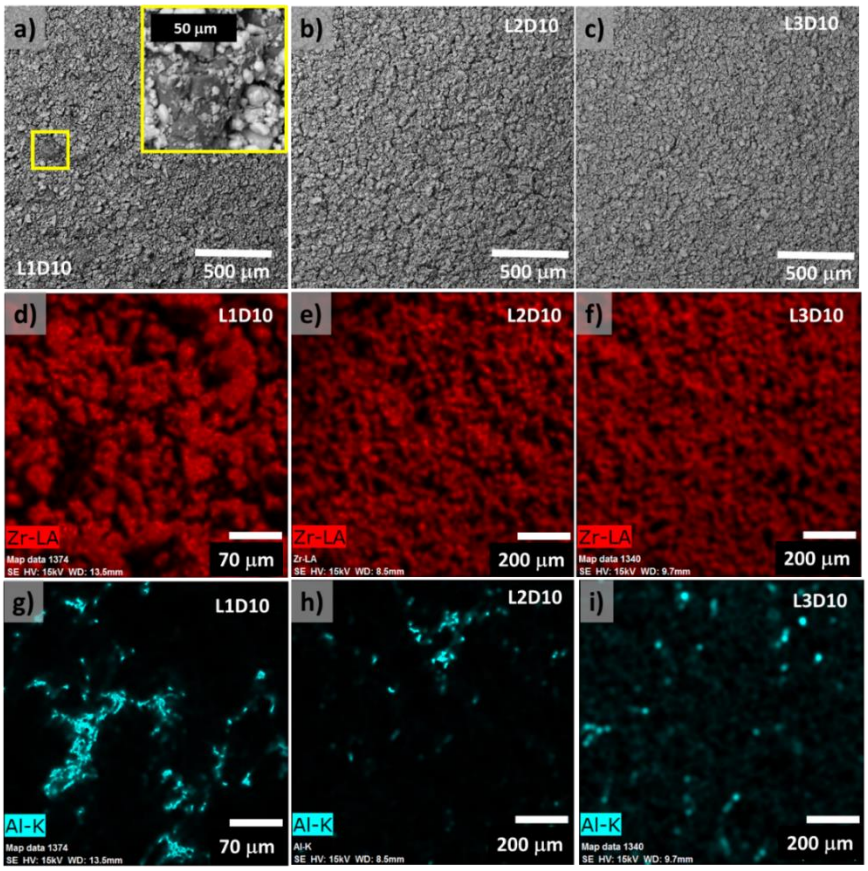

Fig. 4.9. Surface morphology of the produced coatings by the slurry composed of 10% of lanthanum aerogel powder and its former sol; a) L1D10; b) L2D10; c) L3D10; d-i) EDX images of the coatings.

The amount of aerogel on the substrate was significantly improved with the slurry of 20% as can be seen in **Fig. 4.10**. Slight cracks appear after the second deposit and increase to the third as well as the coarsening of the coating being indicative of the higher amount of aerogel powder. Although there are fewer aluminum spots compared to the samples prepared with 10%, some uncoated spots can still be observed as revealed by the EDX images (**Fig. 4.10g-i**).

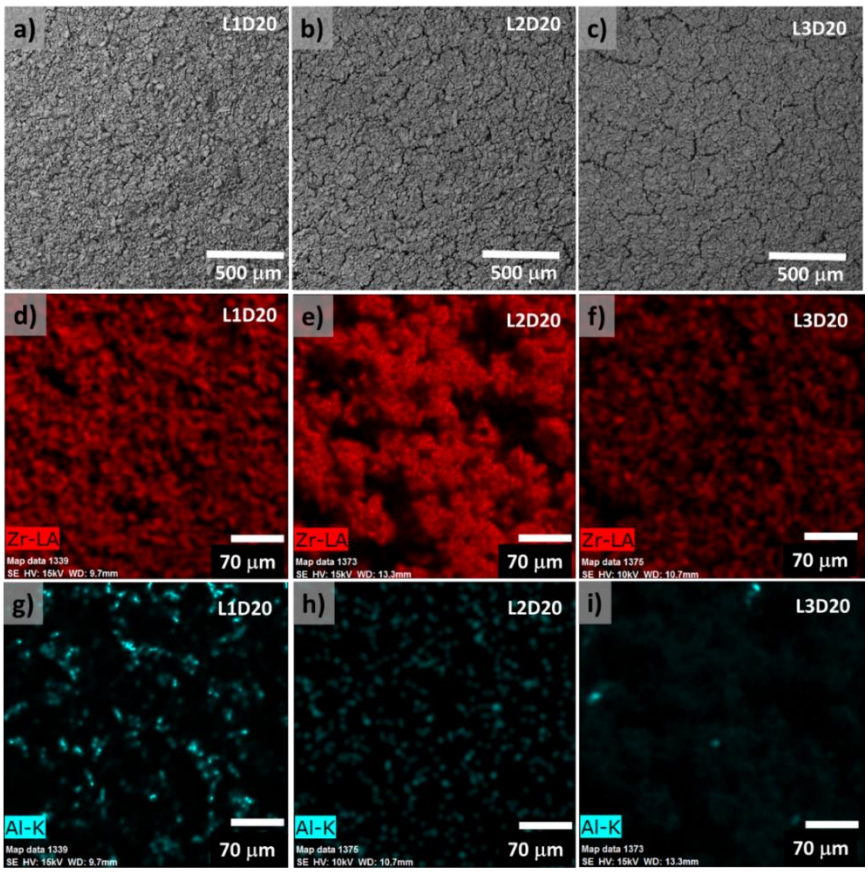

Fig. 4.10. Surface morphology of the produced coatings by the slurry composed of 20% of lanthanum aerogel powder and its former sol; a) L1D20; b) L2D20; c) L3D20; d-i) EDX images of the coatings.

By increasing the amount of powder to 30%, a thick surface formed by aggregates of about 50 µm is obtained from the first deposit (**Fig. 4.11**). A common feature in most of the studied samples is the appearance of cracks (so-called "mud cracks" [38]). There are several factors that favor the presence of cracks in slurry-based coatings such as drying speed, drying temperature, solution composition, deposited amount, and particle size, among others [33,36,38–40]. The higher amount of deposited aerogel powder gave an increasing thickness with the number of depositions from ~100 nm at ~250 nm and the drawbacks of the others methods were avoided as displayed in **Fig. 4.11g-i**.

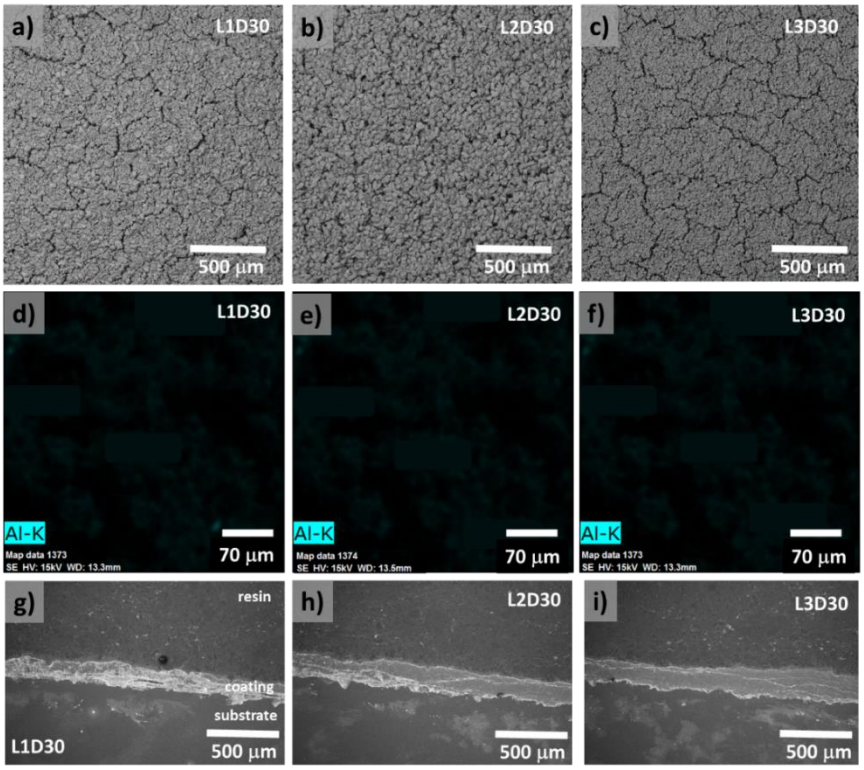

Fig. 4.11. Surface morphology of the produced coatings by the slurry composed of 30% of lanthanum aerogel powder and its former sol; a) L1D30; b) L2D30; c) L3D30; d-f) EDX images of the coatings; g-i) cross-section of the obtained coatings.

4.2.3.1. Heat treatment effect

Based on the thickness of the coating, the sample L3D30 was selected to reproduce onto a Ni-based superalloy substrate to study possible microstructural changes upon calcination. The heating program was set up to 600, 800, and, 1000 °C with a ramp of 1 °C / min^{-1} and dwell time of 30 min. **Fig. 4.12** shows the scanning electron images after calcination at 600 °C (600L3D), 800 °C (800L3D), and 1000 °C (1000L3D). Post calcination, new and more marked cracks appeared. The most affected sample was the one treated at 1000 °C. As can be seen in **Fig. 4.12h**, after the heat treatment at 1000 °C, the aerogel retains its highly porous structure. Similar to its bulk counterpart, the coating preserves the porosity which corroborates the great resistance to sintering. However, unlike the aerogels in bulk form, despite the heat treatment, the coatings did not apparently reveal signs of massive shrinkage as can be seen in **Fig. 4.12c-inset**.

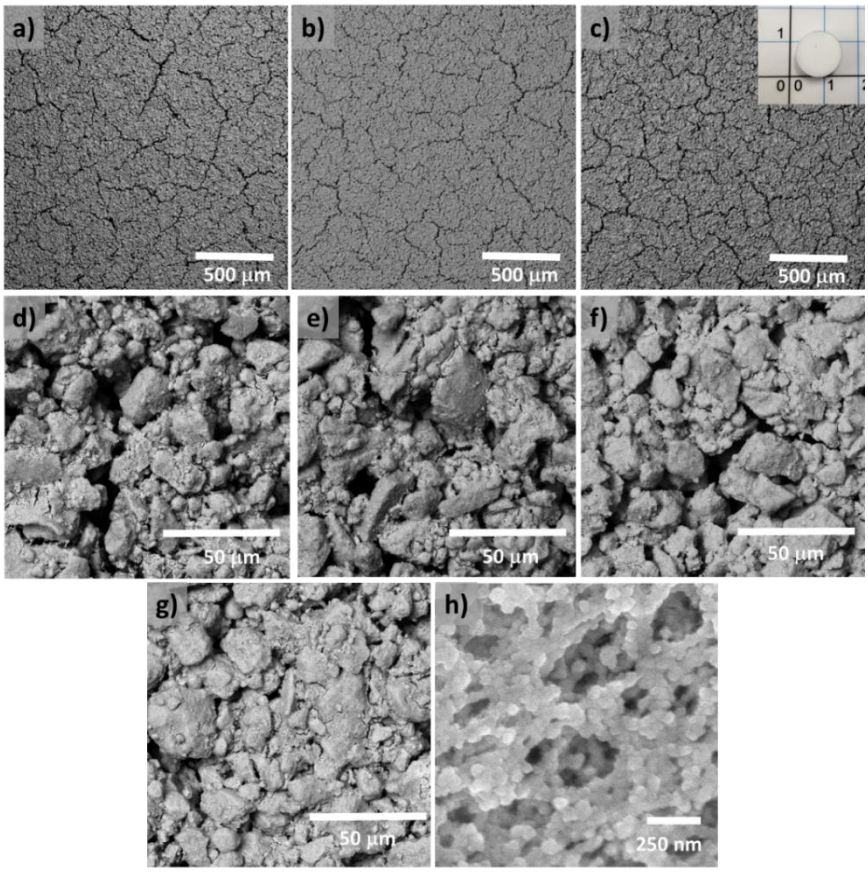

Fig. 4.12. Surface morphology of the L3D30 coating submitted to different calcination temperatures. a) 600L3D; b) 800L3D; c) 1000L3D; d-f) higher magnification detail of the coatings; g) detail of the L3D30 before calcination; h) detail of the 1000L3D coating.

4.2.3.2. Furnace cycling oxidation test: coating performance under simulated operating conditions

For this test, two coated substrates (L2D30 and L3D30) were subjected to successive heating-cooling cycles into a furnace. After the processing, the samples are presented in **Fig. 4.13**. Both samples showed similar behavior. From the macroscopic images is clearly visible that a progressive detachment occurs with the heating-cooling cycles, mostly all the coating has detached out from the substrate after 4 cycles.

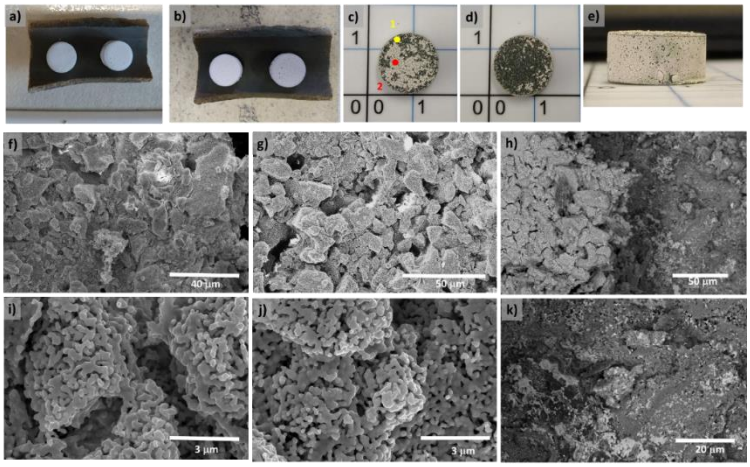

Fig. 4.13. Macroscopic and microscopic images of the L3D30 coatings after 4 heating-cooling cycles at 1100 °C. a-d) Digital photos of the coatings after 1, 2, 3, and 4 cycles, respectively; e) side view of the coating; f-g) low magnification of the L2D30 and L3D30 coatings, respectively; h) aerogel-substrate interface; i-j) high magnification images of the L2D30 and L3D30 coatings, respectively; k) oxide growth. All SEM images were taken after 4 cycles.

Coarsening of the surface coating occurs upon exposition to heating-cooling cycling as revealed by the SEM images. Namely, there is a sintering process producing larger and denser aggregates at the macroscopic level (**Fig. 4.13f-g**). Nonetheless, although sintering of the nanoparticles, the aggregates are highly porous as can be appreciated in **Fig. 4.13i-j**. For porous coatings, this result is very important. Despite the high-temperature treatment, the $La_2Zr_2O_7$ aerogel coating has an enhanced resistance to densification. LZ aerogels proved to maintain the characteristic porous structure of these materials.

5. Conclusion

In this thesis, a systematic study of the physicochemical properties of Zr-based aerogels was carried out. Namely, the synthesis, calcination process, type of aerogel and deposition, must be carefully considered for high-temperature coatings applications. To this purpose, ZrO_2, YSZ, and $Ln_2Zr_2O_7$ (Ln=La^{3+}, Nd^{3+}, Gd^{3+}, and Dy^{3+}) aerogels were successfully synthesized. Throughout the experimental work done can be concluded the following points:

1) A simplified synthetic route allowed obtaining high-purity aerogel materials was found. When zirconium propoxide is involved, the water concentration plays a determinant role in the sol-gel reactions. The incorporation of a disproportionate amount of water can lead to the formation of precipitates or to the development of secondary phases in the final product.

2) According to the proposed reaction mechanism, nitric acid is determinant to control the sol-gel reactions. Insufficient acid results in the partial hydrolysis of the propoxy groups and therefore uncontrolled precipitation occurs. The adequate HNO_3 concentration drives the hydrolysis/condensation reactions to form a free-precipitate wet gel in a few minutes while oversaturation caused complete inhibition of the gelation.
3) By means of the tunable synthesis method, it was possible to prepare either pure ZrO_2, rare-earth-doped aerogels such as YSZ, or 4 new compositions of rare-earth zirconates in the form of aerogels and xerogels such as $La_2Zr_2O_7$, $Nd_2Zr_2O_7$, $Gd_2Zr_2O_7$, and $Dy_2Zr_2O_7$.
4) The calcination has a great impact on the physicochemical properties of the aerogels. Upon calcination, the ZrO_2 and YSZ suffer from almost complete densification losing their porosity in its totality. On the other hand, the $Ln_2Zr_2O_7$ aerogels retain high surface areas at similar calcination conditions.
5) The phase composition varied regarding the material. The ZrO_2 aerogel firstly crystallizes to tetragonal followed by a complex phase transformation pathway determined by the crystallite size in a range of temperatures. In general, excellent phase stability resulted when a trivalent rare-earth ion (Ln^{3+}) which was added to the zirconium oxide structure. Namely, the YSZ experimented an amorphous-to-tetragonal phase transition was found stable from room temperature up to 1200 °C. The phase composition of the $Ln_2Zr_2O_7$ materials is highly dependent on the synthesis and the incorporated rare-earth element. Specifically, regarding the powders (co-precipitation) and xerogels (sol-gel) yielding single-phase pyrochlore ($La_2Zr_2O_7$ and $Nd_2Zr_2O_7$) or fluorite ($Gd_2Zr_2O_7$, $Dy_2Zr_2O_7$) cubic phases. The new system of rare-earth zirconate aerogels resulted in a mixture of $Ln_2Zr_2O_7$ and traces of tetragonal phases. All these phases were stable in studied temperature range up to 1200 °C.
6) The deposition of aerogels as a coating by soft chemistry routes must be performed under strictly controlled conditions. The direct formation of a wet gel onto the substrate surface suffers from extensive shrinkage upon supercritical drying. The combination of shrinkage and adhesion of the aerogel causes tensile stress that yields cracking and detachment of the deposited coating. The magnitude of these stresses seems larger in thick coatings than thinner ones.
7) The coating deposition by means of the formulation of a slurry and 30% wt. of fine aerogel

powder demonstrated to be the most suitable approach in comparison with the solution dip coating and the doctor-blade methods. Mostly all the drawbacks were avoided since there is no evident shrinkage and detaching of the coating.

8) Both bulk and coating $La_2Zr_2O_7$ aerogels demonstrated enhanced thermal stability by the retention of its porous nature upon calcination. Despite certain consolidation of the nanoparticles, the aggregates that built the coating showed several open pores ranges below 1 μm even after continuous heating-cooling cycles at the temperatures higher than 1000 °C.

References

[1] F. Rechberger, M. Niederberger, Synthesis of aerogels: From molecular routes to 3-dimensional nanoparticle assembly, *Nanoscale Horizons*. 2 (**2017**) 6–30. https://doi.org/10.1039/c6nh00077k.

[2] S. Yoon, G.D. Han, D.Y. Jang, J.W. Kim, D.H. Kim, J.H. Shim, Fabrication of yttria-stabilized zirconia aerogel for high-performance thermal barrier coating, *J. Alloys Compd.* 806 (**2019**) 1430–1434. https://doi.org/10.1016/j.jallcom.2019.07.156.

[3] L. Pin, C. Pilgrim, J. Feist, Y. Le Maoult, F. Ansart, P. Lours, Characterisation of thermal barrier sensor coatings synthesised by sol-gel route, *Sensors Actuators, A Phys.* 199 (**2013**) 289–296. https://doi.org/10.1016/j.sna.2013.03.022.

[4] G. Moskal, L. Swadzba, B. Mendala, M. Góral, M. Hetmanczyk, Degradation of the TBC system during the static oxidation test, *J. Microsc.* 237 (**2010**) 450–455. https://doi.org/10.1111/j.1365-2818.2009.03290.x.

[5] I. Smirnova, P. Gurikov, Aerogel production: Current status, research directions, and future opportunities, *J. Supercrit. Fluids*. 134 (**2018**) 228–233. https://doi.org/Https://doi.org/10.1016/j.supflu.2017.12.037.

[6] I. Lázár, I. Fábián, A Continuous Extraction and Pumpless Supercritical CO_2 Drying System for Laboratory-Scale Aerogel Production, *Gels*. 2 (**2016**) 26. https://doi.org/10.3390/gels2040026.

[7] L. Pin, V. Vidal, F. Blas, F. Ansart, S. Duluard, J.P. Bonino, Y. Le Maoult, P. Lours, Optimized sol-gel thermal barrier coatings for long-term cyclic oxidation life, *J. Eur. Ceram. Soc.* 34 (**2014**) 961–974. https://doi.org/10.1016/j.jeurceramsoc.2013.10.013.

[8] J. Fenech, C. Viazzi, F. Ansart, J.P. Bonino, Elaboration of sol-gel coatings from aerogels and xerogels of doped zirconia for TBC applications, *Adv. Mater. Res.* 89–91 (**2010**) 184–189. https://doi.org/10.4028/www.scientific.net/amr.89-91.184.

[9] L. Pin, F. Ansart, J.-P. Bonino, Y. Le Maoult, V. Vidal, P. Lours, Reinforced sol–gel thermal barrier coatings and their cyclic oxidation life, *J. Eur. Ceram. Soc.* 33 (**2013**) 269–276. https://doi.org/10.1016/j.jeurceramsoc.2012.07.037.

[10] A.C. Karaoglanli, T. Grund, A. Turk, T. Lampke, A comparative study of oxidation kinetics and thermal cyclic performance of thermal barrier coatings (TBCs), *Surf. Coatings Technol.* 371 (**2019**) 47–67. https://doi.org/10.1016/j.surfcoat.2018.12.082.

[11] O. Fabrichnaya, H.J. Seifert, T. Ludwig, F. Aldinger, A. Navrotsky, The assessment of thermodynamic parameters in the Al_2O_3-Y_2O_3 system and phase relations in the Y-Al-O system, *Scand. J. Metall.* 30 (**2001**) 175–183. https://doi.org/10.1034/j.1600-0692.2001.300308.x.

[12] G. Soyez, J.A. Eastman, L.J. Thompson, G.-R. Bai, P.M. Baldo, A.W. McCormick, R.J. DiMelfi, A.A. Elmustafa, M.F. Tambwe, D.S. Stone, Grain-size-dependent thermal conductivity of nanocrystalline yttria-stabilized zirconia films grown by metal-organic chemical vapor deposition, *Appl. Phys. Lett.* 77 (**2000**) 1155–1157. https://doi.org/10.1063/1.1289803.

[13] S.K. Gupta, P.S. Ghosh, C. Reghukumar, N. Pathak, R.M. Kadam, Experimental and theoretical approach to account for green luminescence from $Gd_2Zr_2O_7$ pyrochlore: exploring the site occupancy and origin of host-dopant energy transfer in $Gd_2Zr_2O_7$:Eu^{3+}, *RSC Adv.* 6 (**2016**) 44908–44920. https://doi.org/10.1039/c6ra05113h.

[14] S. Dey, J.W. Drazin, Y. Wang, J.A. Valdez, T.G. Holesinger, B.P. Uberuaga, R.H.R. Castro, Radiation tolerance of nanocrystalline ceramics: Insights from yttria stabilized zirconia, *Sci. Rep.* 5 (**2015**) 1–9. https://doi.org/10.1038/srep07746.

[15] K. Sing, The use of nitrogen adsorption for the characterisation of porous materials, *Colloids Surfaces A Physicochem. Eng. Asp.* 187–188 (**2001**) 3–9. https://doi.org/10.1016/s0927-7757(01)00612-4.

[16] B.C. Lippens, J.H. de Boer, Studies on pore systems in catalysts: V. The t method, *J. Catal.* 4 (**1965**) 319–323. https://doi.org/10.1016/0021-9517(65)90307-6.

[17] E.P. Barrett, L.G. Joyner, P.P. Halenda, The Determination of Pore Volume and Area Distributions in Porous Substances. I. Computations from Nitrogen Isotherms, *J. Am. Chem. Soc.* 73 (**1951**) 373–380. https://doi.org/10.1021/ja01145a126.

[18] J. Torres-Rodríguez, J. Kalmár, M. Menelaou, L. Čelko, K. Dvořak, J. Cihlář, J. Cihlař, J. Kaiser, E. Győri, P. Veres, I. Fábián, I. Lázár, Heat treatment induced phase transformations in zirconia and yttria-stabilized zirconia monolithic aerogels, *J. Supercrit. Fluids*. 149 (**2019**). https://doi.org/10.1016/j.supflu.2019.02.011.

[19] M. Thommes, K. Kaneko, A. V. Neimark, J.P. Olivier, F. Rodriguez-Reinoso, J. Rouquerol, K.S.W. Sing, Physisorption of gases, with special reference to the evaluation of surface area and pore size distribution (IUPAC Technical Report), *Pure Appl. Chem.* 87 (**2015**) 1051–1069. https://doi.org/10.1515/pac-2014-1117.

[20] E. Aleshin, R. Roy, Crystal Chemistry of Pyrochlore, *J. Am. Ceram. Soc.* 45 (**1962**) 18–25. https://doi.org/10.1111/j.1151-2916.1962.tb11022.x.

[21] J. Torres-Rodriguez, V. Gutierrez-Cano, M. Menelaou, J. Kaštyl, J. Cihlář, S. Tkachenko, J.A. González, J. Kalmár, I. Fábián, I. Lázár, L. Čelko, J. Kaiser, Rare-Earth Zirconate $Ln_2Zr_2O_7$ (Ln: La, Nd, Gd, and Dy) Powders, Xerogels, and Aerogels: Preparation, Structure, and Properties, *Inorg. Chem.* (**2019**) acs.inorgchem.9b01965. https://doi.org/10.1021/acs.inorgchem.9b01965.

[22] L. Zhou, Z. Huang, J. Qi, Z. Feng, D. Wu, W. Zhang, X. Yu, Y. Guan, X. Chen, L. Xie, K. Sun, T. Lu, Thermal-Driven Fluorite–Pyrochlore–Fluorite Phase Transitions of $Gd_2Zr_2O_7$ Ceramics Probed in Large Range of Sintering Temperature, *Metall. Mater. Trans. A.* 47 (**2016**) 623–630. https://doi.org/10.1007/s11661-015-3234-4.

[23] K. Shimamura, T. Arima, K. Idemitsu, Y. Inagaki, Thermophysical Properties of Rare-Earth-Stabilized Zirconia and Zirconate Pyrochlores as Surrogates for Actinide-Doped Zirconia, *Int. J. Thermophys.* 28 (**2007**) 1074–1084. https://doi.org/10.1007/s10765-007-0232-9.

[24] D. Michel, M.P. y Jorba, R. Collongues, Study by Raman spectroscopy of order-disorder phenomena occurring in some binary oxides with fluorite-related structures, *J. Raman Spectrosc.* 5 (**1976**) 163–180. https://doi.org/10.1002/jrs.1250050208.

[25] S. Wang, W. Li, S. Wang, Z. Chen, Synthesis of nanostructured $La_2Zr_2O_7$ by a non-alkoxide sol–gel method: From gel to crystalline powders, *J. Eur. Ceram. Soc.* 35

(**2015**) 105–112. https://doi.org/10.1016/j.jeurceramsoc.2014.08.032.

[26] F.N. Sayed, V. Grover, K. Bhattacharyya, D. Jain, A. Arya, C.G.S. Pillai, A.K. Tyagi, Sm2-xDyxZr2O7 pyrochlores: Probing order-disorder dynamics and multifunctionality, *Inorg. Chem.* 50 (**2011**) 2354–2365. https://doi.org/10.1021/ic200108u.

[27] I. Lázár, J. Kalmár, A. Peter, A. Szilágyi, E. Győri, T. Ditrói, I. Fábián, Photocatalytic performance of highly amorphous titania–silica aerogels with mesopores: The adverse effect of the in situ adsorption of some organic substrates during photodegradation, *Appl. Surf. Sci.* 356 (**2015**) 521–531. https://doi.org/10.1016/j.apsusc.2015.08.113.

[28] Y.V. Kolen'ko, A.V. Garshev, B.R. Churagulov, S. Boujday, P. Portes, C. Colbeau-Justin, Photocatalytic activity of sol–gel derived titania converted into nanocrystalline powders by supercritical drying, *J. Photochem. Photobiol. A Chem.* 172 (**2005**) 19–26. https://doi.org/10.1016/j.jphotochem.2004.11.004.

[29] H. Li, G. Li, J. Zhu, Y. Wan, Preparation of an active SO_4^{2-}/TiO_2 photocatalyst for phenol degradation under supercritical conditions, *J. Mol. Catal. A Chem.* 226 (**2005**) 93–100. https://doi.org/10.1016/j.molcata.2004.09.028.

[30] R. Moussaoui, K. Elghniji, M. ben Mosbah, E. Elaloui, Y. Moussaoui, Sol–gel synthesis of highly TiO2 aerogel photocatalyst via high temperature supercritical drying, *J. Saudi Chem. Soc.* 21 (**2017**) 751–760. https://doi.org/10.1016/j.jscs.2017.04.001.

[31] A. Díaz-Parralejo, A. Macías-García, E.M. Cuerda-Correa, R. Caruso, Influence of the type of solvent on the textural evolution of yttria stabilized zirconia powders obtained by the sol–gel method: Characterization and study of the fractal dimension, *J. Non. Cryst. Solids*. 351 (**2005**) 2115–2121. https://doi.org/10.1016/j.jnoncrysol.2005.03.046.

[32] A. Díaz-Parralejo, A. Macías-García, J. Sánchez-González, M.Á. Díaz-Díez, E.M. Cuerda-Correa, Influence of the experimental parameters on the synthesis process of yttria-doped zirconia sol–gel films, *Surf. Coatings Technol.* 204 (**2010**) 2257–2261. https://doi.org/10.1016/j.surfcoat.2009.12.015.

[33] L. Scandola, S. Latorrata, R. Matarrese, C. Cristiani, I. Nova, Effect of thickness and cracking phenomena on the photocatalytic performances of Ti/TiO_2 photoanodes

produced by dip coating, *Mater. Chem. Phys.* 234 (**2019**) 1–8. https://doi.org/10.1016/j.matchemphys.2019.05.074.

[34] A.C. Pierre, G.M. Pajonk, Chemistry of Aerogels and Their Applications, *Chem. Rev.* 102 (**2002**) 4243–4266. https://doi.org/10.1021/cr0101306.

[35] M. Seyedjalali, M.R. Madani, Silica aerogel thick film, an alternative to micromachined air gap for thermal insulation, *Electron. Lett.* 51 (**2015**) 849–850. https://doi.org/10.1049/el.2015.0088.

[36] P.C. Innocenzi, M. Guglielmi, M. Gobbin, P. Colombo, Coating of metals by the sol-gel dip-coating method, *J. Eur. Ceram. Soc.* 10 (**1992**) 431–436. https://doi.org/10.1016/0955-2219(92)90018-9.

[37] C.-T. Wang, C.-L. Wu, I.-C. Chen, Y.-H. Huang, Humidity sensors based on silica nanoparticle aerogel thin films, *Sensors Actuators B Chem.* 107 (**2005**) 402–410. https://doi.org/10.1016/j.snb.2004.10.034.

[38] E. Santanach Carreras, F. Chabert, D.E. Dunstan, G.V. Franks, Avoiding "mud" cracks during drying of thin films from aqueous colloidal suspensions, *J. Colloid Interface Sci.* 313 (**2007**) 160–168. https://doi.org/10.1016/j.jcis.2007.03.076.

[39] A. Torabi, T.H. Etsell, P. Sarkar, Dip coating fabrication process for micro-tubular SOFCs, *Solid State Ionics*. 192 (**2011**) 372–375. https://doi.org/10.1016/j.ssi.2010.09.050.

[40] P. Xu, A.S. Mujumdar, B. Yu, Drying-Induced Cracks in Thin Film Fabricated from Colloidal Dispersions, *Dry. Technol.* 27 (**2009**) 636–652. https://doi.org/10.1080/07373930902820804.